



Obrabotka metallov -

Metal Working and Material Science

Journal homepage: http://journals.nstu.ru/obrabotka_metallov



Structural and mechanical properties of stainless steel formed under conditions of layer-by-layer fusion of a wire by an electron beam

Vasily Fedorov^{1, a, *}, Aleksandr Rygin^{2, b}, Vasily Klimenov^{1, c}, Nikita Martyushev^{1, d}, Anatolii Klopotov^{2, 3, e}, Irina Strelkova^{1, f}, Sergey Matrenin^{1, g}, Andrey Batranin^{1, h}, Valentina Deryusheva^{1, i}

¹ National Research Tomsk Polytechnic University, 30 Lenin ave., Tomsk, 634050, Russian Federation

² Tomsk State University of Architecture and Building, 2 Solyanaya Sq., Tomsk, 634003, Russian Federation

³ National Research Tomsk State University, 36 Lenin ave., Tomsk, 634050, Russian Federation

^a  <https://orcid.org/0000-0002-5164-5875>,  fedorov@tpu.ru, ^b  <https://orcid.org/0000-0001-5664-8234>,  alexandr.rygin@gmail.com,
^c  <https://orcid.org/0000-0001-7583-0170>,  klimenov@tpu.ru, ^d  <https://orcid.org/0000-0003-0620-9561>,  martjushev@tpu.ru,
^e  <https://orcid.org/0000-0002-3690-0436>,  klopotovaa@tsuab.ru, ^f  <https://orcid.org/0000-0002-2222-2865>,  strelkova@tpu.ru,
^g  <https://orcid.org/0000-0002-2188-8120>,  mstv@tpu.ru, ^h  <https://orcid.org/0000-0001-9678-2905>,  batranin@tpu.ru,
ⁱ  <https://orcid.org/0000-0002-2116-3891>,  vderusheva@tpu.ru

ARTICLE INFO

Article history:

Received: 02 September 2021

Revised: 16 September 2021

Accepted: 23 September 2021

Available online: 15 December 2021

Keywords:

Additive technologies
 Electron beam surfacing
 Stainless steel
 Coarse austenitic steel

Funding

This research was supported by TPU development program.

Acknowledgements

Research were conducted at core facility "Structure, mechanical and physical properties of materials".

ABSTRACT

Introduction. As of today, additive technologies are among the most promising methods to manufacture various parts. They allow producing parts of complex shapes and provide their quality structure. The quality of the structure formed depends on numerous parameters: equipment type, its operation mode, materials, shielding medium, etc. Large international companies producing 3D-printers provide technological guidelines for working on it. Such guidelines include the information on the manufacturers of raw materials (printing powders), products their equipment can work with and the operation modes that should be used with such powders. These parameters should be investigated to use it on the domestic equipment developed within the framework of research programs and import substitution programs. The researchers and developers of 3D-printing equipment frequently run into a problem of using currently available raw materials for obtaining parts possessing minimal porosity, uniform structure and mechanical properties similar to that of at least cast blanks. One of the widely used materials for 3D-printing is stainless steel. It has high corrosion resistance, which reduces the requirements to the medium in which 3D printing is carried out. Manufactured stainless steel products have a good combination of strength and plastic characteristics. **The aim of the study** is to obtain stainless steel specimens possessing minimal number of micro- and macro-defects and uniform structure by the method of wire arc additive manufacturing using an electron-beam setup developed at Tomsk Polytechnic University. **The methods to study** the AISI 308LSi stainless steel 3D-printed specimens are as follows: XRD analysis, tomography, chemical analysis, metallographic analysis, microhardness testing. **Results and discussion.** It is established that the AISI 308LSi stainless steel specimens manufactured using the electron-beam 3D-printing setup contain no macro-defects in the bulk of the specimens. There are small microdefects represented by residual gas pores with the dimensions of no more than 5.2 μm. The microstructure of the specimens is formed close to that of coarse-grained cast austenite steels and consists of columnar grains of the γ-Fe austenite matrix and high-temperature ferrite. The interfaces between the wire layers are not pronounced; however, there are small differences in phase composition. Based on the analysis of the results obtained, it is established that the use of electron-beam 3D-printing for the manufacture of parts from AISI 308LSi steel gives a structure similar to cast austenitic steels. Macro-defects do not appear, and the number of gas pores is small.

For citation: Fedorov V.V., Rygin A.V., Klimenov V.A., Martyushev N.V., Klopotov A.A., Strelkova I.L., Matrenin S.V., Batranin A.V., Deryusheva V.N. Structural and mechanical properties of stainless steel formed under conditions of layer-by-layer fusion of a wire by an electron beam. *Obrabotka metallov (tekhnologiya, oborudovanie, instrumenty) = Metal Working and Material Science*, 2021, vol. 23, no. 4, pp. 111–124. DOI: 10.17212/1994-6309-2021-23.4-111-124. (In Russian).

* Corresponding author

Fedorov Vasily Viktorovich, Laboratory manager
 National Research Tomsk Polytechnic University,
 30 Lenin ave.,
 634050, Tomsk, Russian Federation
 Tel.: 8 (3822) 606006, e-mail: fedorov@tpu.ru

Introduction

Additive Technologies (*AT*), or 3D-printing with metals, is the most rapidly growing sector of Additive Manufacturing (*AM*). *ATs* allow manufacturing the parts that cannot be produced by other methods; they are less material-consuming as compared to other technologies and reduce production costs [1–4]. It is important in 3D-printing with metals that the solid-state digital model of the part is combined with the software of the printing device itself. The production of parts involves layer-by-layer deposition welding using various heat sources and raw materials. Such parts are demanded by aerospace industry, medical, energy and transport engineering. Examples of such parts are custom-tailored medical implants, turbine blades, special coolers with internal channels, fasteners, reticulated structures and trusses with optimal weight-to-strength ratio for space equipment, etc. It is remarkable that with the help of *ATs* it is possible to manufacture parts with a specific composition and properties. The methods of layer-by-layer deposition welding of metal powders on a substrate with direct melting of the material in the zone of high-energy beam have gained the widest application in additive manufacturing of metal products. The most often used high-energy sources are lasers and electron-beam guns [1–6]; in some cases they are arc discharges and gas-discharge plasmas [7, 8]. It should be noted that in recent years, along with selective methods of fusion of materials in additive technologies, methods of layer-by-layer melting are increasingly used in the direct deposition of a material in the zone of a high-energy laser or electron beam. The feeding of the material to be deposited (a wire or a rod) is used quite often [7–13]. In such cases, electron-beam or arc sources are used as heat sources [7, 10–13]. These sources allow to carry out the 3D-printing process with high productivity and give low porosity of the printed products. In *ATs*, various metals, alloys and compositions are used as raw materials [4, 14]. However, the mostly used are stainless steels and titanium alloys. The potential of such parts is outstanding. The implementation of titanium alloys is accompanied with a number of issues, such as the requirement of welding in vacuum. Welding in vacuum has higher efficiency when electron beam is used [1, 5, 10–13]. Austenitic stainless steels are welded well by both laser sintering and electron-beam welding [1, 4, 12, 14–17].

The structure of parts from stainless steels and titanium alloys is in direct dependence on the method they are manufactured. The parameters of printing equipment have direct impact on the strength, hardness, heat resistance, heat stability and other properties [18]. When printing steel parts by layer-by-layer deposition welding, an ordered crystalline structure forms. In comparison with traditional methods of manufacturing (casting, shaping of metals) new phases and defects may occur, chemical composition and structure may change at different scales [4]. Changes in the structure of steel parts manufactured by *AT* methods give them changes in properties such as elasticity modulus, strength, viscosity, fatigue resistance, creep. As a result, such changes affect the corrosion resistance of steel and the part as a whole [15–17]. Despite the considerable number of works on 3D-printing with steels, there are few works investigating steel specimens at different scales, including those with implementation of non-destructive testing methods. The discontinuities and pores are typical defects in parts 3D-printed layer-by-layer. To remove such defects, a variety of post-processing treatment methods are used. Post-processing complicates the manufacturing process and increases the cost of the final product. At the same time, the study of the pore formation process in different 3D-printing modes has shown that the porosity can be reduced without additional treatment just by selecting suitable modes [19]. In recent time, different non-destructive testing methods have been used to study porosity in 3D-printed parts [13, 20]. Printed titanium alloy parts are often tested using nanoindentation. This method is used to study the properties of titanium alloys formed using plasmas [21], electron-beam melting of powders [22] and electron-beam additive processing [23]. Nanoindentation is also used to study materials produced by contact welding of titanium and gold alloys [24].

Therefore, the development of new methods and technics for manufacturing parts from stainless steels is one of the key directions of modern manufacturing development. The development of proprietary setups and complexes for additive manufacturing and *AT*-based production are of high priority [12].

The work is aimed at manufacturing stainless-steel specimens possessing uniform structure and minimal amount of macro- and micro-defects using Wire Arc Additive Manufacturing (*WAAM*) method on an electron-beam setup developed at Tomsk Polytechnic University.

Materials and Methods

The specimens were printed on the electron-beam setup developed at Tomsk Polytechnic University [15] using a stainless steel wire. The accelerating voltage was 30 kV and the beam current varied from 15 to 20 mA (depending on the distance from the substrate). Thus, the power input varied from 450 to 600 W. The first three layers were printed at an accelerating voltage of 30 kV and beam current of 20 mA. High current was used to heat up the substrate. The next three layers were formed at 30 kV and 17 mA to reduce the specimen heat up rate. Consequent layers were formed at 30 kV and 15 mA to reject generated heat. Focused beam (with a diameter of 150 μm) was moving along circular sweep with a diameter of 4 mm. The beam movement frequency was 1,000 Hz. The wire was fed into the sweep zone, while the specimen geometry was formed by moving the bed along three axes. The hatching distance was 4 mm, while the layer height was 0.8 mm. The specimen was moved in a zig-zag pattern. The appearance of the specimen and the build-up scheme are presented in Figure 1.

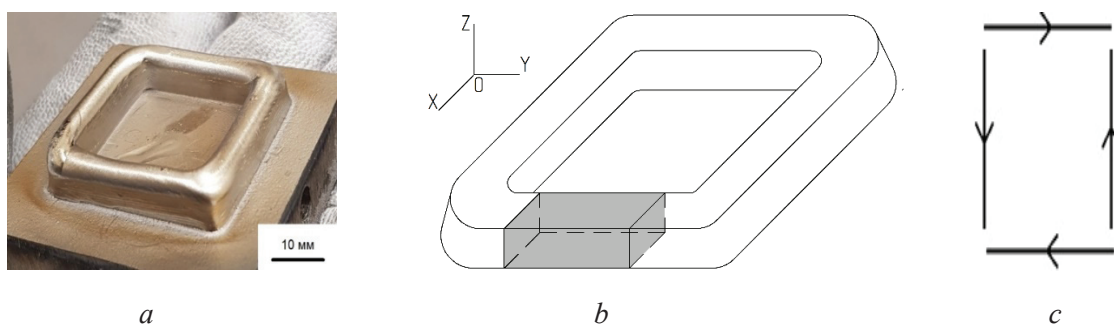


Fig. 1. Appearance of the specimen (a), specimen cutting area (b) and specimen build-up scheme (c)

The raw material for the blank to be produced by electron-beam-assisted *WAAM* was *AISI 308LSi* steel wire. The chemical composition of the wire is presented in Table 1.

Table 1

Chemical composition of the raw material

Fe [%] (balance)	C [%]	Mn [%]	Si [%]	Cr [%]	Ni [%]	P [%]	S [%]
64.82...69.37	0.03	1.4...2.1	0.65...1.0	19.5...21.0	9.0...11.0	0.03	0.02

The specimens for consequent studies were cut by the electrospark method from the blank to form geometrically valid parallelepiped specimens with dimensions of 5×5×10 mm.

Tomographic investigation to control micro- and macro-defects of the specimens was carried out on an *Orel-MT* X-ray computer microtomograph. The device was equipped with an *XWT 160-TC* X-ray tube and *PaxScan-2520V* detector panel with a positioning control system. The specimens were scanned with the following parameters: accelerating voltage – 130 kV, current – 27 μA , resolution – 11.3 μm , number of projections – 1,200, scanning step – 0.3, copper filter – 2 mm. The tomographic reconstruction was performed using *NRecon* Reconstruction Software (*Bruker Micro-CT*). After reconstruction, the tomograms were segmented to obtain two models: the specimen material and internal porosity. In addition, morphological properties of single pores were studied: volume, typical diameter and sphericity. The segmentation and analysis were carried out in *CTanalyser* software (*Bruker Micro-CT*).

The microstructure was studied on an *Axio Observer* metallographic microscope (*Carl Zeiss*) with 1,000x magnification. The microscope comes with software for quantitative analysis of the phase and structural composition of alloys. The transverse and longitudinal metallographic sections were prepared by grinding on polishing papers with different grit sizes. The sections were finished on a fabric with an

aqueous suspension of chrome oxide. The microstructure was controlled after etching of the microsection. The section was etched by the solution of concentrated nitric (HNO_3) and hydrochloric (HCL) acids at a volumetric ratio of 1:3.

XRD analysis was aimed at determining the parameters of elementary cells of compositions and phase composition with the help of a *Shimadzu XRD-7000S* X-ray diffractometer located in the Scientific and educational innovative center “Nanomaterials and Nanotechnologies” at Tomsk Polytechnic University (School of Advanced Manufacturing Technologies) at an accelerating voltage and current of 40.0 kV and 30.0 mA, respectively. The source of X-ray $Cu_{K\alpha}$ radiation (wavelength of 1.5406 Å) was *Cu* anode. The measurement range was from 10 to 80 degrees, the scanning speed was 2.0 deg/min with a step of 0.02 degrees. The structural state was identified by the *Rietveld* method. The benchmark lattices were represented by the crystallographic data from *COD* database.

The hardness distribution along the specimen height was recorded using an automatic complex based on a *Duramin-5* microhardness meter at indentation load of 25 grams (245.17 mN) and a spacing of 250 µm from the lower edge of the specimen and between the indentations.

The hardness testing along the blank height was performed on a *NanoIndenter G200* setup (Materials Science Division, School of Advanced Manufacturing Technologies, NR TPU). The specimen was indented by a Berkovich pyramid at constant load, scheme and spacing between the indentations. The largest load reached 250 mN with a spacing between the sections of 100 µm and with a spacing from the substrate of 50 µm to eliminate edge effects of hardness measurement.

The mechanical compression tests were performed on an *Instron* testing rig in accordance with *GOST 25.503-97*. The load was applied to the longest side of the specimens with a rate of 5 mm/min.

During the tests, *AISI 308LSi* specimens did not fail; the deformation was primarily plastic.

Results and Discussion

In this work, a batch of specimens was manufactured on an electron-beam 3D-printer [16] developed and produced at Tomsk Polytechnic University. The specimens were studied by several methods (metallographic, tomographic, XRD analysis, etc.).

Computer tomography with a resolution of 11.3 µm has demonstrated no micro- and macro-defects on the surface and in the bulk of the specimen (Fig. 2). This result testifies to avoided occurrence of extended defects due to the use of electron-beam-assisted *WAAM*.

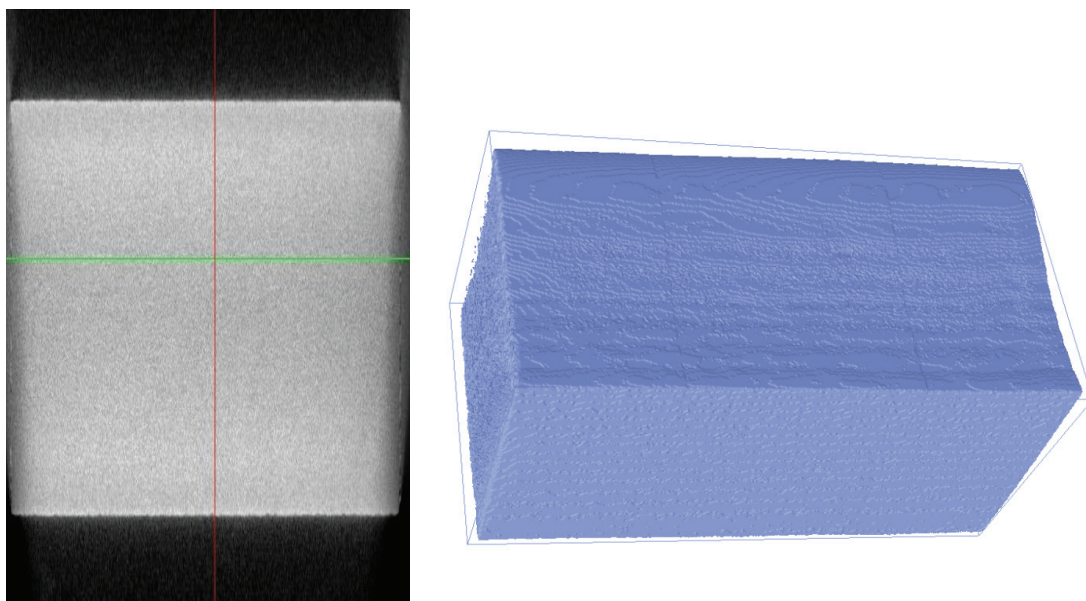


Fig. 2. Tomography of *AISI 308LSi* specimens manufactured by *WAAM*

The microstructure of the samples has a shape characteristic of coarse-grained cast austenite steels. It consists of columnar grains growing along the height of the wire layers (Fig. 3a). The average size of the austenitic grain is $d = 150\text{--}200\ \mu\text{m}$ (Fig. 3b). During consistent layer-by-layer welding of the wire, each consequent layer was formed due to fusion of the metal with a previous layer due to partial heating of metal up to the melting temperature. Such fusion mode revealed no evident interfaces between the layers. However, different parts of the blank were characterized by nonuniformity of the phase composition and different mechanical properties.

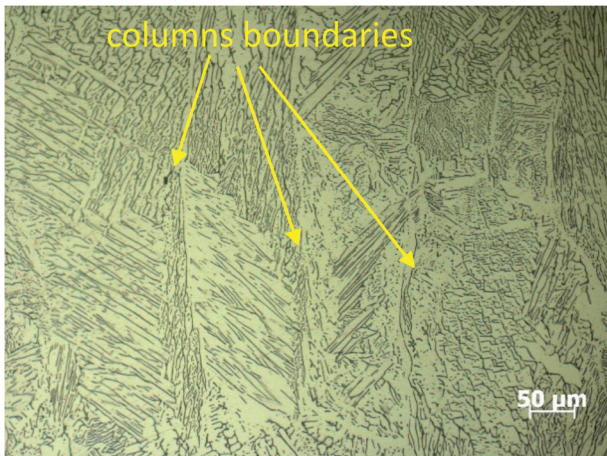


Fig. 3a. Columnar grains in the longitudinal section of the specimen

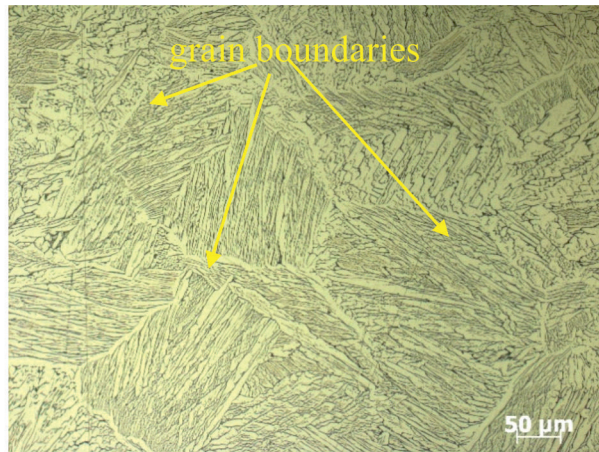


Fig. 3b. Grain structure in the cross-section of the specimen

Two-phase structure was revealed inside the columnar grains both in longitudinal and transverse directions. The two-phase nature is characterized by the γ -Fe-based austenitic matrix with FCC-lattice (bright color) and inclusions from δ -Fe-based high-temperature ferrite with BCC lattice of various shape (dark color). The microstructure analysis allowed distinguishing three typical morphological types of ferrite inclusions: needle-like, vermicular and granular (Fig. 5).

The specimens have a columnar large-grain microstructure oriented along the growth direction. Epitaxial growth leads to the formation of grains with a width from 70 to 230 μm and length from 180 to 630 μm . The microstructure of the formed grains forms an austenitic matrix, including needle-like, granular and vermicular forms of δ -ferrite. There are no macro-scale nonuniformities in the form of boundaries between deposited metal layers. The studies of the surface at a different scale by the method of scanning electron microscopy allowed for unveiling defects in the form of residual gas pores formed during printing of the blank. The dimensions of gas pores in the metal structure varied between 0.5 and 5.2 μm (Figs. 4, a and b).

The shape and size of the δ -Fe inclusions are different in different grains. (Fig. 5, a). There are austenite grains with needle-like ferrite and negligible amount of grain ferrite (Fig. 5, b). In addition, austenite grains with vermicular ferrite and a large amount of grain ferrite were identified (Fig. 5, d). Low carbon content in austenitic steel of the WAAM-specimens under study did not lead to the formation of metal carbides; however, it contributed to the formation of grain ferrite with grain size $d = 1\ \mu\text{m}$. According to [15, 16], such chemical composition of austenitic steel (Table 1) provides crystallization starting from δ -Fe-ferrite formation from liquid melt in line with the mechanism of peritectic transformation. The amount and form of ferrite inclusions is determined by different cooling rate of the deposited wire layers. Under high cooling rate of a new wire layer, the diffusion of the major alloying elements (Ni , Cr) that induce phase transformation of δ -Fe into austenite is almost absent; the size and amount of ferrite increases, while its major share has vermicular or needle-like form. The decrease in the previous layer cooling rate and high temperature allows diffusion of the alloying elements (Ni , Cr). The diffusion leads to the dissolution of δ -Fe. That is why the boundaries of formed columnar grains are austenitic having a low amount of granular δ -Fe (Fig. 5, c).

The XRD analysis (Fig. 6) has shown the following phase composition of the specimens: the main phase is austenite (γ -Fe, FCC) with a unit cell parameter of 3.5807 Å, while the second phase is low-

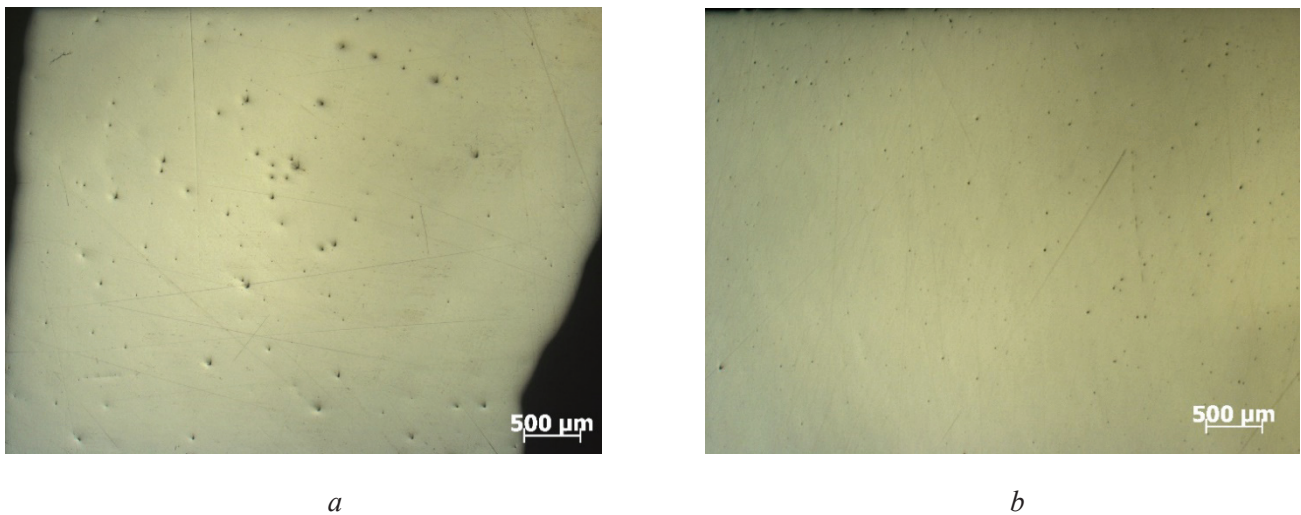


Fig. 4. Surface of the sections of *WAAM*-obtained *AISI 308LSi* steel specimens: longitudinal section (a), cross section (b)

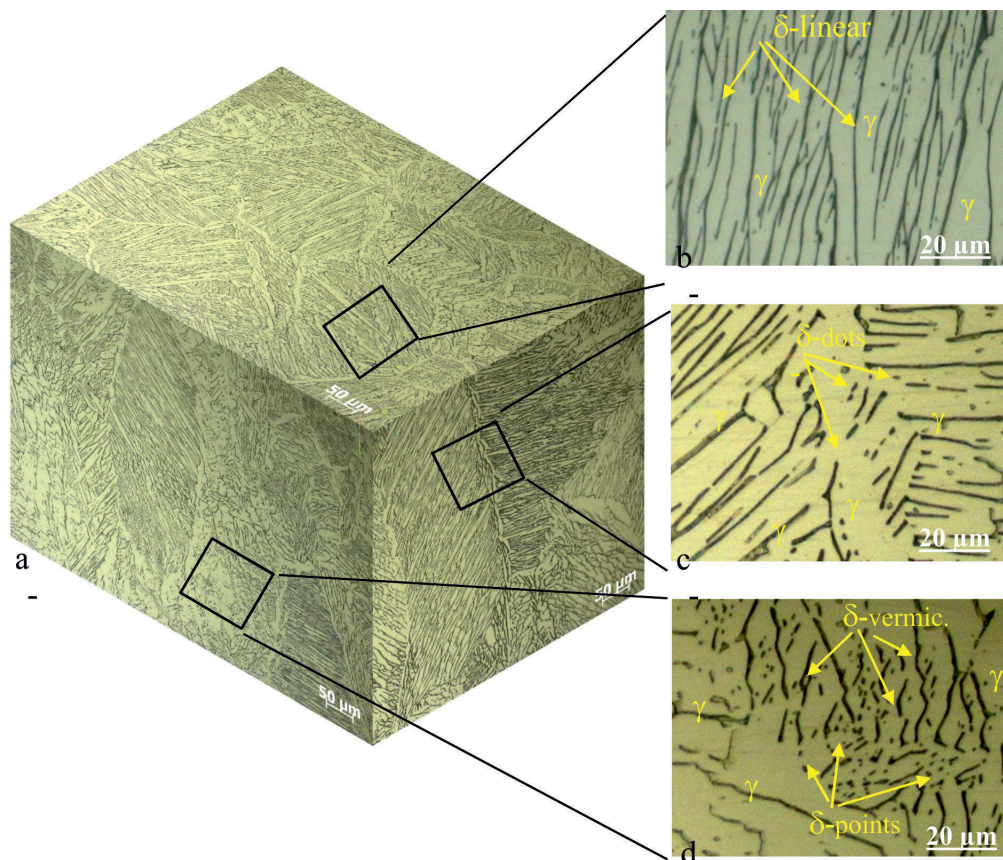


Fig. 5. Microstructure of three surfaces of the sample

temperature stabilized δ -*Fe*-based phase with *BCC* and a unit cell parameter of 2.8613 Å. According to the X-ray fluorescence analysis, the mass fractions for austenitic and ferrite phases have amounted to 79 and 21±3 wt% , correspondingly.

The diffraction patterns from different planes of the *WAAM*-specimens are presented in Figs. 7 and 8. The *XRD* analysis has revealed that the matrix phase is a γ -*Fe*-based solid solution with *FCC* lattice. The second phase is a α -*Fe*-based solid solution with *BCC* lattice. The results are in line with the *Cr-Ni-Fe* triple system (Fig. 9) [25].

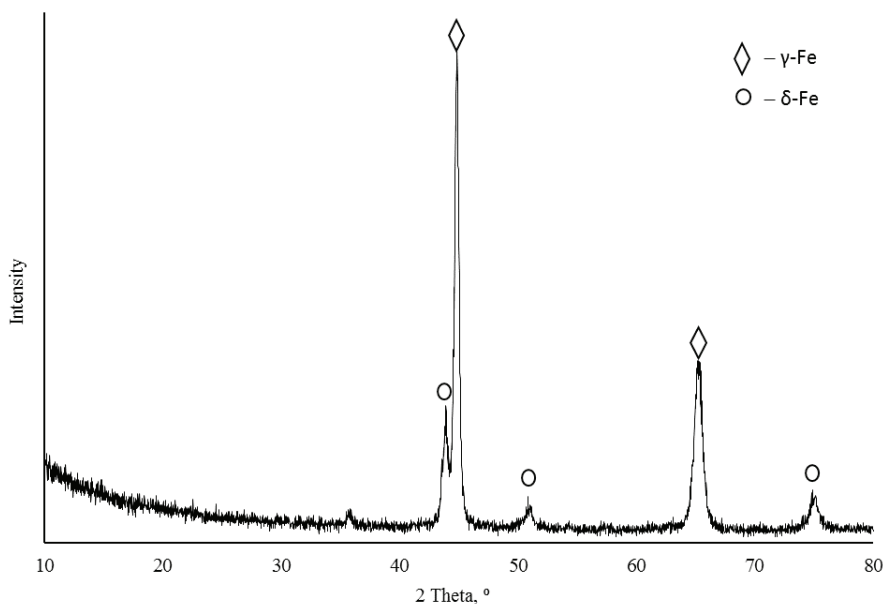


Fig. 6. XRD analysis of WAAM-obtained AISI 308LSi steel specimens

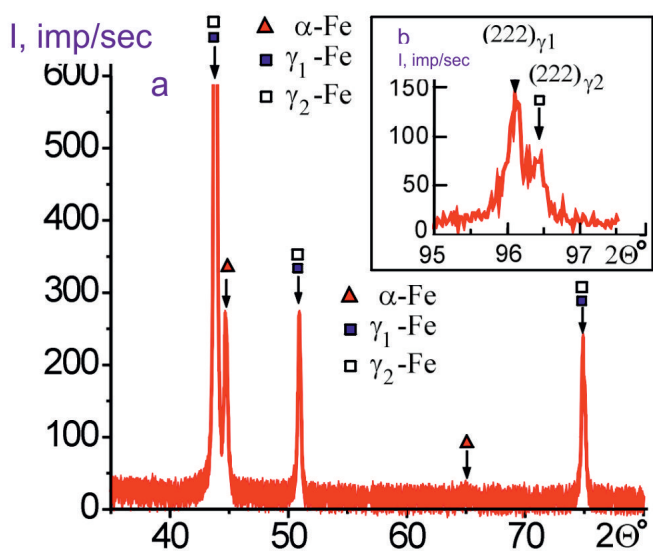


Fig. 7. Diffraction patterns of the specimen with the plane parallel to the sintered layers (a) and a fragment of the diffraction pattern with structural line (222) of the γ -(Fe,Cr,Ni) phase (b)

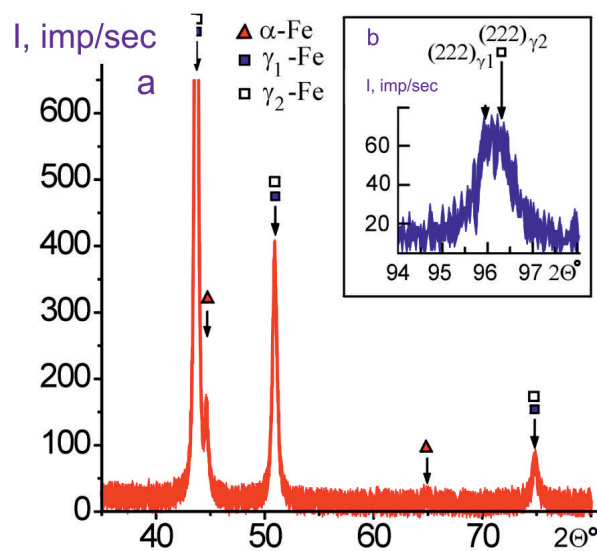


Fig. 8. Diffraction patterns of the specimen with the plane perpendicular to the sintered layers (a) and a fragment of the diffraction pattern with structural line (222) of the γ -(Fe, Cr, Ni) phase (b)

In this diagram, the asterisk denotes the location of the three-component alloy with the chemical composition of the steel under study. During the crystallization of an alloy with such a composition under conditions of nonequilibrium processes, as in the case of layer-by-layer formation of an ingot by electron-beam deposition welding, a two-phase mixture from two solid solutions based on BCC and FCC lattices can form: γ -(Fe,Ni,Cr) and α -(Cr,Ni,Fe).

The profile of γ -(Fe,Ni,Cr) structure lines was analyzed in the diffraction patterns from the high-angle region 2Θ . It was established that the profile of structural lines (222), (400) and (331) of the γ -(Fe,Ni,Cr) phase from the high-angle region 2Θ can be represented as a superposition of two lines from the phases with close lattice parameters. The revealed complex profile of the structural lines of γ -(Fe,Ni,Cr) phase testifies to nonuniform chemical composition on the specimen surface comprised of compositions based

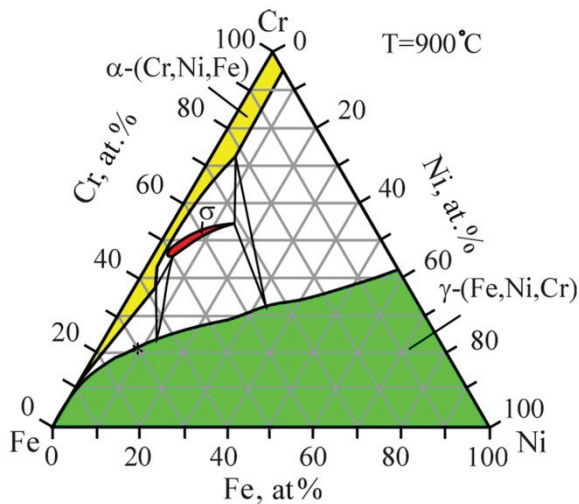


Fig. 9. Isothermal section at 900 °C of the *Fe-Cr-Ni* triple system [25]

regions, as compared to the regions with austenitic matrix (100 HV) (Figs. 10 and 11). The received data demonstrate that the δ -*Fe* phase is harder than the γ -*Fe*-based austenitic phase. When manufacturing parts and structures with higher strength, the presence of δ -*Fe* will negatively affect the durability under long static loads causing higher concentration of stresses that promote cracking. To increase the durability of parts, the negative effect of δ -*Fe* can be reduced by preliminary thermomechanical treatment or consequent hardening thermal treatment.

The diagram, depicted in Fig. 11 shows no evident alteration of hardness along the height from the substrate to the upper deposited layer in both longitudinal and transverse sections. The average hardness in longitudinal section (*XOZ*) was 187 ± 7 HV; that of transverse section (*YOZ*) was 200 ± 9 HV.

According to the results of nanoindentation, the average value of elastic aftereffect amounted to $7.24 \pm 0.63\%$.

Conclusions

It was established that the *AISI 308LSi* stainless steel specimens manufactured using the electron-beam 3D-printing setup contain no macro-defects in the bulk of the specimens. There are small micro-defects in the form of residual gas pores occurred during growing of the blank. The diameter of the gas pores is less than 5.2 μm . The microstructure of the specimens is close to that of large-grain cast austenitic steels.

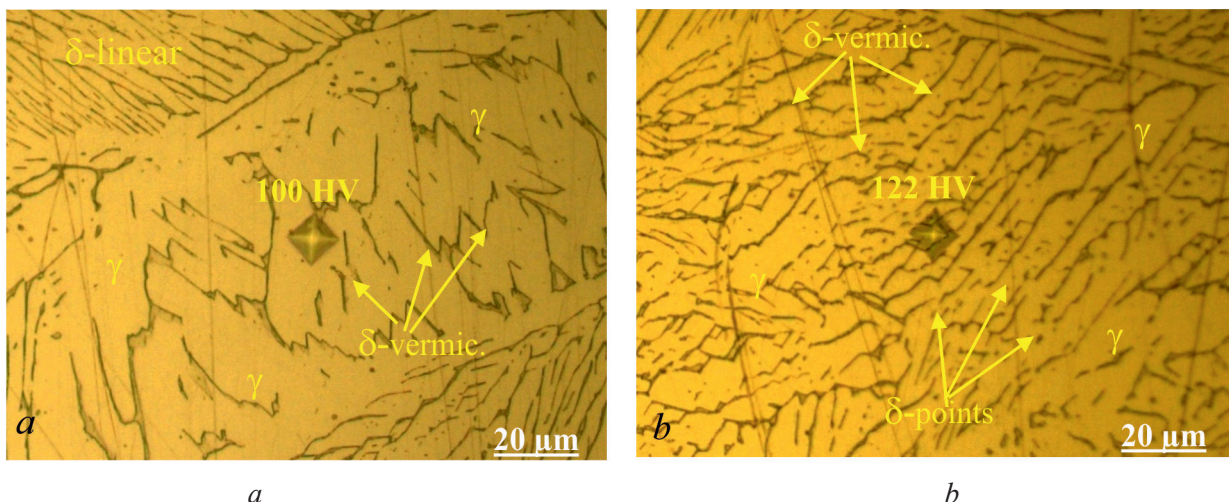


Fig. 10. Microhardness in the zone of γ -*Fe* (a) and the zone of $(\gamma+\delta)$ *Fe* (b)

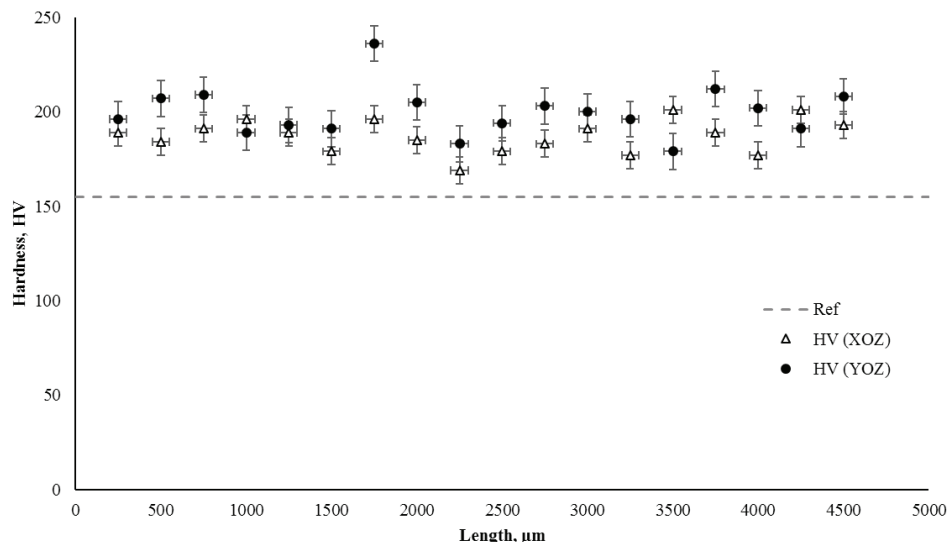


Fig. 11. Microhardness measurements along cross sections *XOZ* and *YOZ*

The structure primarily contains columnar grains directed along the deposition of layers along the height. The structural studies have revealed two-phase composition. The main phase is an austenitic matrix based on γ -*Fe* with an *FCC*-lattice and inclusions of high-temperature ferrite δ -*Fe* with a *BCC* lattice of various shapes. The needle-like, granular and vermiculite forms of δ -ferrite were identified. The sharp interface between the wire layers is not pronounced; however, there are small differences in the phase composition. These alterations affect mechanical properties. Microhardness tests have shown that it alters within 10%.

The results allowed establishing that the use of electron-beam 3D-printing for manufacturing parts from *AISI 308LSi* steel provides the structure similar to that of cast austenitic steels. There are no macro-defects and the number of gas pores is small.

References

- Murr L.E. Metallurgy of additive manufacturing: examples from electron beam melting. *Additive Manufacturing*, 2015, vol. 5, pp. 40–53. DOI: 10.1016/j.addma.2014.12.002.
- Milevski J.O. *Additive manufacturing of metals: from fundamental technology to rocket, nozzles, medical implants and custom jewelry*. Cham, Springer, 2017. 351 p. ISBN 978-3-319-58205-4.
- Zhang Y., Wu L., Guo X., Kane S., Deng Y., Jung Y.-G., Lee J.-H., Zhang J. Additive manufacturing of metallic materials: a review. *Journal of Materials Engineering and Performance*, 2018, vol. 27, iss. 1, pp. 1–13. DOI: 10.1007/s11665-017-2747-y.
- DebRoy T., Mukherjee T., Wei H.L., Elmer J.W., Milewski J.O. Metallurgy, mechanistic models and machine learning in metal printing. *Nature Reviews Materials*, 2020, vol. 6, pp. 48–68. DOI: 10.1038/s41578-020-00236-1.
- Edwards P., O’Conner A., Ramulu M. Electron beam additive manufacturing of titanium components: properties and performance. *Journal of Manufacturing Science and Engineering*, 2013, vol. 135, iss. 6, p. 061016. DOI: 10.1115/1.4025773.
- Tavlovich B., Shirizly A., Katz R. EBW and LBW of additive manufactured Ti6Al4V products. *Welding Journal*, 2018, vol. 97, iss. 6, pp. 179–190. DOI: 10.29391/2018.97.016.
- Peleshenko S., Korzhyk V., Voitenko O., Khaskin V., Tkachuk V. Analysis of the current state of additive welding technologies for manufacturing volume metallic products. *Eastern-European Journal of Enterprise Technologies*, 2017, vol. 3/1, iss. 87, pp. 42–52. DOI: 10.15587/1729-4061.2017.99666.
- Wang J., Pan Z., Wei L., He S., Cuiuri D., Li H. Introduction of ternary alloying element in wire arc additive manufacturing of titanium aluminide intermetallic. *Additive Manufacturing*, 2019, vol. 27, pp. 236–245. DOI: 10.1016/j.addma.2019.03.014.
- Chekir N., Sixsmith J.J., Tollett R., Brochu M. Laser wire deposition of a large Ti-6Al-4V space component. *Welding Journal*, 2019, vol. 28, iss. 6, pp. 172–180.
- Taminger K.M., Hafley R.A. Electron beam freeform Fabrication for cost effective near-net shape manufacturing. *NATO/RTO AVT-139 Specialists’ Meeting on Cost Effective Manufacture via Net Shape Processing*, Amsterdam, 2006, p. 16.

11. Savchenko N.L., Vorontsov A.V., Utyaganova V.R., Eliseev A.A., Rubtsov V.E., Kolubaev E.A. Osobennosti strukturno-fazovogo sostoyaniya splava Ti-6Al-4V pri formirovani izdelii s ispol'zovaniem elektronno-luchevoi provolochnoi additivnoi tekhnologii [Features of the structural-phase state of the alloy Ti-6Al-4V in the formation of products using wire-feed electron beam additive manufacturing]. *Obrabotka metallov (tekhnologiya, oborudovanie, instrumenty) = Metal Working and Material Science*, 2018, vol. 20, no. 4, pp. 60–71. DOI: 10.17212/1994-6309-2018-20.4-60-71.
12. Fedorov V.V., Klimenov V.A., Batranin A.V., Ranga P. Development of electron-beam equipment and technology for additive layer-wise wire cladding. *AIP Conference Proceedings*, 2019, vol. 2167, p. 020097. DOI: 10.1063/1.5131964.
13. Klimenov V.A., Fedorov V.V., Slobodyan M.S., Pushilina N.S., Strelkova I.L., Klopotov A.A., Batranin A.V. Microstructure and compressive behavior of Ti-6Al-4V alloy built by electron beam free-form fabrication. *Journal of Materials Engineering and Performance*, 2020, vol. 29, iss. 11, pp. 7710–7721. DOI: 10.1007/s11665-020-05223-9.
14. Simar A., Godet S., Watkins T.R. Highlights of the special issue on metal additive manufacturing. *Materials Characterization*, 2018, vol. 143, pp. 1–4. DOI: 10.1016/j.matchar.2018.06.013.
15. Tarasov S.Yu., Filippov A.V., Savchenko N.L., Fortuna S.V., Rubtsov V.E., Kolubaev E.A., Psakhie S.G. Effect of heat input on phase content, crystalline lattice parameter, and residual strain in wire-feed electron beam additive manufactured 304 stainless steel. *The International Journal of Advanced Manufacturing Technology*, 2018, vol. 99, pp. 2353–2363. DOI: 10.1007/s00170-018-2643-0.
16. Tarasov S.Yu., Filippov A.V., Shamarin N.N., Shamarin N., Fortuna S.V., Maier G.G., E.A. Kolubaev. Microstructural evolution and chemical corrosion of electron beam wire-feed additively manufactured AISI 304 stainless steel. *Journal of Alloys and Compounds*, 2019, vol. 803, pp. 364–370. DOI: 10.1016/j.jallcom.2019.06.246.
17. Xu X., Ganguly S., Ding J., Guo S., Williams S., Martina F. Microstructural evolution and mechanical properties of maraging steel produced by wire + arc additive manufacture process. *Materials Characterization*, 2018, vol. 143, pp. 152–162. DOI: 10.1016/j.matchar.2017.12.002.
18. Kostina M.V., Krivorotov V.I., Kostina V.S., Kudrashov A.E., Muradyan S.O. Osobennosti khimicheskogo sostava i strukturno-fazovogo sostoyaniya, obuslovlivshie snizhenie korrozionnoi stoikosti detalei iz stali 18Cr-10Ni [Features of chemical composition and structural-phase state decreasing corrosion resistance of parts from 18Cr-10Ni steel]. *Izvestiya vysshikh uchebnykh zavedenii. Chernaya metallurgiya = Izvestiya. Ferrous Metallurgy*, 2021, vol. 64, pp. 217–229. DOI: 10.17073/0368-0797-2021-3-217-229. (In Russian).
19. Gong H., Rafi K., Gu H., Janaki Ram G.D., Starr T., Stucker B. Influence of defects on mechanical properties of Ti-6Al-4V components produced by selective laser melting and electron beam melting. *Materials and Design*, 2015, vol. 86, pp. 545–554. DOI: 10.1016/j.matdes.2015.07.147.
20. Aleshin N.P., Grigo'rev M.V., Shchipakov N.A., Prilutskii M.A., Murashov V.V. Applying nondestructive testing to quality control of additive manufactured parts. *Russian Journal of Nondestructive Testing*, 2016, vol. 52, iss. 10, pp. 600–609. DOI: 10.1134/S1061830916100028.
21. Barberi F., Otani C., Lepienski C., Urruchi W., Maciel H., Petraconi G. Nanoindentation study of Ti6Al4V alloy nitride by low intensity plasma jet process. *Vacuum*, 2002, vol. 67, iss. 3, pp. 457–461. DOI: 10.1016/S0042-207X(02)00231-2.
22. Karlsson J., Snis A., Engqvist H., Lausmaa J. Characterization and comparison of materials produced by Electron Beam Melting (EBM) of two different Ti-6Al-4V powder fractions. *Journal of Materials Processing Technology*, 2013, vol. 213, iss. 12, pp. 2109–2118. DOI: 10.1016/j.jmatprotec.2013.06.010.
23. Ladany L., Roy L. Mechanical behavior of Ti-6Al-4V manufactured by electron beam additive fabrication. *ASME 2013 International Manufacturing Science and Engineering Conference*, Madison, WI, 2013. DOI: 10.1115/MSEC2013-1105.
24. Klimenov V., Slobodyan M., Ivanov Yu., Kiselev A., Matrenin S. Metallurgy of a Ti-Au alloy synthesized by controlled electric resistance fusion. *Intermetallics*, 2020, vol. 127, p. 106968. DOI: 10.1016/j.intermet.2020.106968.
25. Lee B.J. A thermodynamic evaluation of the Fe-Cr-Ni System. *Journal of the Korean Institute of Metals and Materials*, 1993, vol. 31, iss. 4, pp. 480–489.

Conflicts of Interest

The authors declare no conflict of interest.